# Drug repurposing of allophenylnorstatine containing HIV-protease inhibitors against SARS-CoV-2 M$^{pro}$: Insights from Molecular Dynamics simulations and binding free energy estimations.

**Jiban Jyoti Dash[1], Priyanka Purohit[1], Jules Tshishimbi Muya[2,3], Biswa Ranjan Meher[1]***

[1] *Computational Biology and Bioinformatics Laboratory,*
*PG Department of Botany, Berhampur University, Berhampur, Odisha-760007, INDIA*

[2] *Department of Chemistry, Hanyang University, Seoul, South Korea*

[3] *Research Centre for Theoretical Chemistry and Physics in Central Africa,*
*University of Kinshasa, Faculté of Science, DR Congo.*

***Corresponding Author:**
     **Dr. Biswa Ranjan Meher**
     **Computational Biology and Bioinformatics Laboratory,**
     **Department of Botany, Berhampur University,**
     **Berhampur, Odisha, India.**
     **E-mail: brm.bot@buodisha.edu.in**

**Abstract:**

Coronavirus-2 Main protease (SARS-CoV-2 M$^{pro}$), one of the most vital enzymes of the new coronavirus-2 (SARS-CoV-2) and a crucial target for drug discovery, has been battered with numerous types of drugs/inhibitors. Regrettably, till date there is no any potential drugs or effective inhibitors available to combat its action. Based on the reports of HIV-protease inhibitors can be applied against the SARS by targeting the SARS-CoV-1 M$^{pro}$, we have chosen few clinically trialed experimental HIV-protease inhibitors (KNI-764 or JE-2147, KNI-227 & KNI-272) and a variant JE2-CH3, to examine their binding affinities with SARS-CoV-2 M$^{pro}$ and to assess their potential to check for a possible drug candidate against the protease. Here, we have chosen a methodology to understand the rational elucidation of the binding mechanism of these four inhibitors to SARS-CoV-2 M$^{pro}$ by merging molecular docking, molecular dynamics (MD) simulation, and MM-PBSA based free energy calculations. Our estimations disclose that JE-2147 is highly effective ($\Delta G_{Bind}$ = -14.95 kcal/mol) compared to JE2-CH3 (- 11.19 kcal/mol), KNI-227 (-13.93) and KNI-272 (-12.84) against SARS-CoV-2 M$^{pro}$. The increase in $\Delta G_{Bind}$ for JE-2147 comparative to other three inhibitors arises due to an increased favorable van der Waals interactions ($\Delta E_{vdw}$) and decreased solvation energies ($\Delta G_{solv}$) between the inhibitor and viral protease. Residue decomposition analysis and hydrogen-bonding pattern confirms binding affinities of the inhibitors crucial for the interactions. Binding contributions of important residues (His41, Met49, Cys145, His164, Met165, Pro168, Gln189 etc.) from the active site or near the active site regions with ≥ 1.0 kcal/mol suggest a potent binding of the inhibitors. It is anticipated that the current study of binding interactions of these APNS containing inhibitors can pitch some valuable insights to design the significantly effective anti-SARS-CoV-2 M$^{pro}$ drugs.

**Keywords**: Coronavirus; SARS-CoV-2 M$^{pro}$; Drug discovery; Molecular Dynamics simulation, Binding energy; MM-PBSA.

# 1. Introduction:

Coronavirus disease 2019 (COVID-19) pandemic has been a mounting public health concern and has created a global emergency health situation, mainly due to the infection of a novel coronavirus, recognized as severe acute respiratory syndrome - coronavirus 2 (SARS-CoV-2) leading to fever,

cough, difficulty in breathing and pneumonia with severe respiratory distress. Starting from December, 2019 this outbreak has been spread from the city of Wuhan, China to almost every corners of the world [Zhou *et. al.* 2020; Wu *et. al.* 2020]. Later on March 11th, 2020, WHO (World Health Organization) declared the outbreak as a global pandemic based on the alarming levels of spread and severity with a fatality rate of about ~ 4%. However, the fatality rate increased by ~7.0% as of 31st May, with 3,67,255 deaths from around 59,39,234 cumulative cases globally. In the current scenario, COVID-19 treatment with presently marketed antivirals has been miserly failed. The spread of the virus globally, deficiency of an explicit cure and the urgent condition has been an acute problem and a challenging issue for the human community, which necessitates usage of entire scientific assets to treat this curse. The progression of a successful chemotherapy for SARS-CoV-2 infection entails an improved understanding of the viral life cycle to explicate probable targets and, thus, to accomplish vital information for the rational design of antiviral agents. Hence, there is an urgent requirement to develop potent and active drugs/medications which can be available, accessible and suitable for practice of peoples most in need.

The coronavirus-2 or SARS-CoV-2 genome translates four structural proteins namely small envelope protein (E), spike glycoprotein (S), matrix glycoprotein (M), and nucleocapsid protein (N) [Reddy *et. al.* 2003]. Over and above the four structural genes, two proteases: (i) papain-like protease (PLP) and (ii) 3-Chymotrypsin-Like protease (3CLpro) or the main (Mpro) protease required for the maturation of coronaviruses, which co-translationally cleaves the two polypeptides into mature non-structural proteins (NSPs) [Lim *et. al.* 2000] that is crucial for the viral life cycle, making it an eye-catching target of anti-COVID drug development [Xia and Kang 2011; Lu *et al.* 2006]. The viral main protease Mpro, consists of three domains (I, II & III: Domain I (amino acid residues 8-101); Domain II (amino acid residues 102 - 184); Domain III (amino acid residues 201-306) and a long loop (185–200) connecting domain II and III) and belongs to the superfamily of cysteine proteases with a catalytic dyad of the conserved residues His41 and Cys145. The substrate-binding site of the Mpro is shaped by a cleft amongst domains I and II (Figure 1).
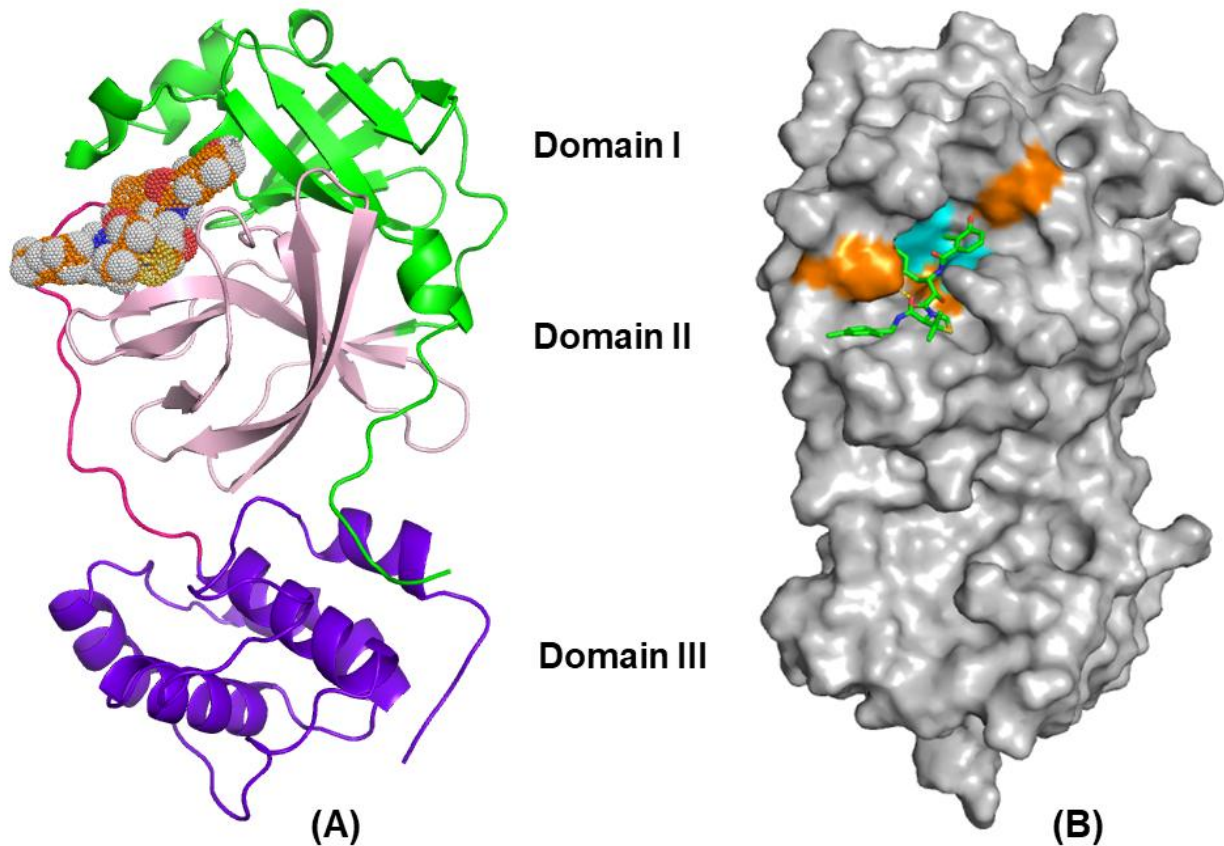
**Figure 1**: Schematic structure of the SARS-CoV-2 M$^{pro}$ (A) showing it's three different domains I, II and III. The active site is situated between the cleft of domain I and II. The structural features are shown by color, where Domain-I in green, Domain-II in light pink, Domain-III in purple blue and a long loop (185-200) is in magenta. The peptide-like inhibitor/ligand is represented as dot-sphere model in orange color. (B) Main protease (M$^{pro}$) structure bound to a ligand in its active site region (Surface view). Cyan region shows the active catalytic dyad residues (His41 and Cys145) and the orange region shows the active site interacting residues to the ligand.

Even though the SARS-CoV-2 M$^{pro}$ crystal structure offers profound understanding into the viral life cycle and enable for selecting possible anti-COVID-19 drugs, not any official drugs have been found to commendably hinder the virus until now. Ever since the development of this pandemic, many reports has been filed to claim that FDA approved experimental anti-viral inhibitors, and/or natural products can be utilized against the SARS-CoV-2 M$^{pro}$ [Joshi *et al.* 2020; Muralidharan *et al.* 2020; Ton et. al. 2020; Elmezayen *et al.* 2020; Khan *et al.* 2020; Abraham Peele *et. al.,* 2020; Lobo-Galo *et. al.* 2020; Chen *et. al.* 2020; Umesh *et al.* 2020; Mahanta *et. al.* 2020; Das *et al.* 2020; Enmozhi *et al.* 2020; Rajib *et al.* 2020; Sk. *et al.,* 2020; Wahedi *et al.,* 2020]. It has also been described that the HIV-1 protease inhibitors can be used against SARS-CoV protease [Zhang *et al.,* 2004; Yamamoto *et. al.,* 2004; Nukolkarn *et. al.* 2008] and thereby can act as anti-COVID-19

drugs by targeting SARS-CoV-2 $M^{pro}$ [Sang *et. al*, 2020; Wang *et. al*, 2020]. Owing to the reports on HIV-protease inhibitors can be applied against the SARS by targeting the SARS-CoV-1 $M^{pro}$, a few groups already tested the currently marketed anti-HIV drugs through *in silico* mode [Sang *et. al*, 2020; Wang *et. al*, 2020]. Kynostatin, the conformationally constrained peptide derivatives are allophenylnorstatine (APNS)-containing HIV-protease inhibitors, and effective against a varied range of HIV-1, HIV-2, SIV, and numerous clinical HIV-1 strains *in vitro*, which might have the capabilities to act against the SARS-CoV-2 $M^{pro}$ and can be repurposed as a potential drug molecule. In the current study, we have repurposed a sets of peptidomimetic HIV-protease inhibitors (JE-2147, JE2147-CH3, KNI-227 and KNI-272) containing APNS, an exclusively unnatural amino acid (Figure 2) against the SARS-CoV-2 $M^{pro}$ to assess their potential to develop proven drugs for COVID-19 therapy through docking, molecular dynamics (MD) simulations and molecular mechanics Poisson-Boltzmann surface area (MM-PBSA) based binding free energy calculations.

JE-2147, belonging to the APNS-based dipeptide, is an experimental HIV-1 protease inhibitor and has potent antiviral activities *in vitro* demonstrating decent oral bioavailability and plasma pharmacokinetic profiles [Yoshimura *et al.* 1999]. Our previous MD studies also demonstrate the potentiality of JE-2147 against HIV-1 protease activities [Bandyopadhyay & Meher, 2006; Dash *et. al.* 2020]. JE2-CH3, the methylated JE-2147, is a variant of the JE-2147 where a methyl group (-CH3) is added to the P2' position of the compound, also exhibits a potentially significant inhibition of HIV-1 protease *in silico* [Dash *et. al.* 2020]. Due to the increased binding efficiency of JE2-CH3 to HIV-1 protease as compared to the normal JE-2147, we proposed to assess the binding interactions of the same against SARS-CoV-2 $M^{pro}$. KNI-227 and KNI-272, are structurally constrained inhibitors containing allophenylnorstatine, has been revealed to be selective and effective inhibitors of HIV-protease, with an inhibitory constant ($K_i$) of 5.5 pM, and to have strong anti-HIV activity with low cytotoxicity [Kageyama, *et al.*, 1993]. The difference exists between the two compounds is with the presence of a dimethylthioproline moiety in KNI-227 as compared to the thioproline in KNI-272. The molecular interactions between all these inhibitors and SARS-CoV-2 $M^{pro}$ is being studied in detail and analyzed for a possible anti-COVID-19 drug development.
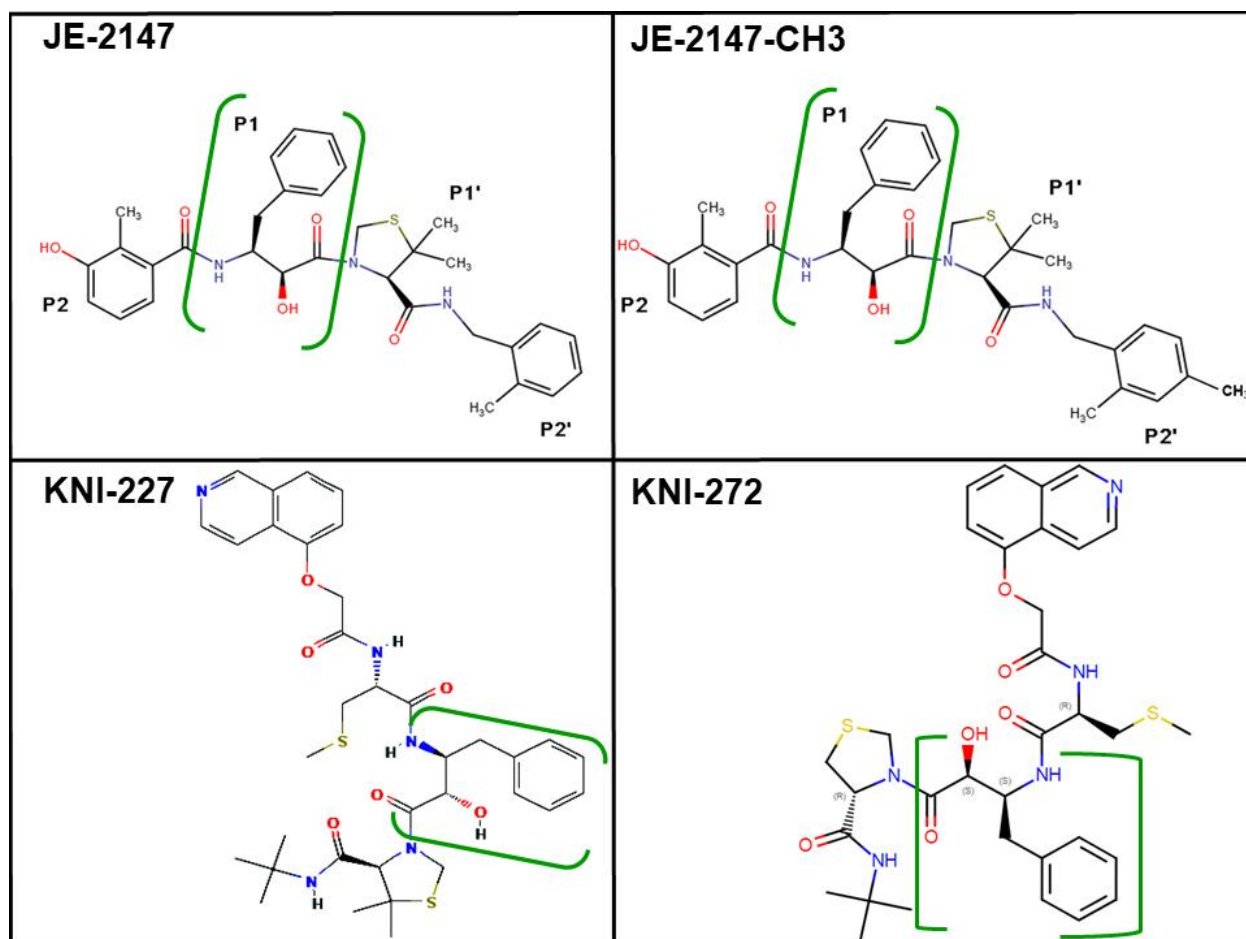
**Figure 2**: 2D Molecular structure of the HIV-protease inhibitors (JE-2147, JE2147-CH3, KNI-227 and KNI-272) containing allophenylnorstatine, which are studied against the SARS-CoV-2 M$^{pro}$. The moiety allophenylnorstatine is labeled with a square bracket in color green. For inhibitors JE-2147 and JE2147-CH3, different sub-structural moieties are represented as P1, P2, P1' and P2'.

## 2. Theory and Methods:

### 2.1. Modeling Ligand-Protease complex through docking:

Crystal structure of the SARS-CoV-2 M$^{pro}$ bound to the N3 inhibitor was acquired from the protein Data Bank (PDB) PDB id: 6LU7 [Jin *et. al.* 2020]. The structure of the apo SARS-CoV-2 M$^{pro}$ was achieved by removing the N3 from the active site of the viral protease. The HIV-protease inhibitor JE-2147 was isolated from PubChem with CID: 446837, which was then modified to add a methyl (-CH3) group in its P2' position to create a methylated variant of the inhibitor JE2-CH3, that has relatively more binding affinity for HIV-1 protease as compared to the standard JE-2147 [Dash *et. al.* 2020]. KNI-272, and KNI-227 are a group of tripeptide HIV-protease inhibitors that has been experimented as a promising candidates as anti-AIDS drugs, is also selected as inhibitors,

were isolated from the PubChem with CID: 60927 and 65012, respectively. All the inhibitors/ligands were then converted to PDBQT format by adding polar hydrogens using Autodock Tools (ADT) -1.5.6 (MGL Tools) [Morris *et al.* 2009]. Again, the ADT-1.5.6 was used to desolvate the protein by removing the water molecules from the crystal protein (6LU7) and polar hydrogens were added to prepare the PDBQT format of the macromolecule. The docking algorithm was then employed to trace the ideal conformation of the ligands in the active site of SARS-CoV-2 M$^{pro}$, which was performed by Autodock Vina [Trott *et al.* 2010] and the binding poses interactions were visualized by Biovia Discovery Studio [www.3dsbiovia.com]. The finest docked structure (protease-inhibitor complexes) with highest negative docking score were then selected to advance for MD simulations and MM-PBSA based binding free energy estimations.

## 2.2. System setups

Charges of all the four ligands (JE-2147, JE2-CH3, KNI-227 and KNI-272) were calculated via restrained electrostatic potential (RESP) procedure [Bayly *et al.*,1993] at the Hartree-Fock/6-31G* once minimizing the molecule at the AM1 semi-empirical level [Dewar, *et al.,*1985]. GAFF force field [Wang *et. al.*, 2004] parameters are assigned for the ligands using the Antechamber module in AMBER18 suite [Case, *et al.* 2018]. The Leap module was used to add all the missing hydrogens. The *ff14SB* [Maier *et al.* 2015] force field was used with TIP3P water models [Jorgensen *et al.*,1983]. The system solvation was done by the TIP3P water models in the periodic box of size holding > 10,000 number of water molecules. A cutoff of 10Å was set to discard water molecules beyond the cutoff from the protein surface. The system was neutralized by adding an appropriate number of Na$^+$ counter ions. For Lennard-Jones interactions, a default cutoff was set to 8.0Å. The particle mesh Ewald (PME) scheme was used to estimate the long-range electrostatic interactions [Essmann *et al.,* 1995]. Constant temperature and pressure situations in the simulations were accomplished by pairing the system to a Berendsen's thermostat and Barostat [Berendsen *et al.*,1984]. The SHAKE [Ryckaert *et al.*,1977] algorithm was employed to restrain all bonds containing hydrogens.

## 2.3. Molecular Dynamics (MD) Simulation

The system was minimized applying restraints (30kcal/mol/Å$^2$) to every heavy atoms of the complex for 10,000 steps with successive 2nd stage minimization of the complete backbone atoms and Cα atoms, respectively, for 10,000 steps for each. The temperature of the system was achieved

to 300K with an interruption of 50K for 10ps with a 1 fs time step. Force constant of 30 kcal/mol/Å$^2$, was employed to restrain the protein atoms keeping the ligand unrestrained and move freely. Next, in the 3rd stage of successive minimization, the force constant was shortened by 10kcal/mol/Å$^2$ in every step to attain the unrestrained structure in three phases of 10,000 steps with all atoms free at the NVT ensemble. Additional 150ps was used to equilibrate the system without any restraints. Temperature, pressure, energies and global RMSDs all used in combination to validate the system's stability. The complexed trajectories for all the four SARS-CoV-2 M$^{pro}$/inhibitors were elongated for 5.0 nanoseconds (ns) using AMBER 18 package with 1 fs time step for the MD production run.

## 2.4. MM-PBSA calculations

Binding free energies of the ligands to the SARS-CoV-2 M$^{pro}$ were calculated using the MM-PBSA.py [Miller III *et. al.*, 2012] tool implemented in AMBER18. We used the MM-PB/GBSA methodology in our previous studies on HIV-1 protease [Meher and Wang, 2012; Meher and Wang, 2012; Meher and Wang, 2015; Meher *et. al.,* 2020] and on Dengue virus NS2B/NS3 protease systems [Purohit *et. al.* 2020] and here we recycled the same procedure.

For each complex, an aggregate number of 500 snapshots were extracted from the complete 5.0 ns trajectories with an intermission of 10 ps. The MM-PBSA method can be briefed as follows.

$$\Delta \textbf{\textit{G}}_{\textbf{Bind}} = \Delta \textbf{\textit{E}}_{\textbf{MM}} + \Delta \textbf{\textit{G}}_{\textbf{solv}} - \text{T} \Delta \textbf{\textit{S}} \dots\dots\dots\dots\dots\dots\dots\dots\dots\dots\dots\dots\dots\dots\dots\dots\dots\dots \text{[4]}$$

Where $\Delta G_{Bind}$ is the binding free energy in solution comprising of the molecular mechanics energy ($\Delta E_{MM}$), the solvation free energy ($\Delta G_{solv}$) and the structural entropy effect to binding ($-T\Delta S$) in the gas phase. $\Delta E_{MM}$ can be expressed as:

$$\Delta \textbf{\textit{E}}_{\textbf{MM}} = \Delta \textbf{\textit{E}}_{\textbf{vdw}} + \Delta \textbf{\textit{E}}_{\textbf{ele}} \quad \dots\dots\dots\dots\dots\dots\dots\dots\dots\dots\dots\dots\dots\dots\dots\dots\dots\dots\dots\dots \text{[5]}$$

Where $\Delta E_{vdw}$ and $\Delta E_{ele}$ correspond to the van der Waals and electrostatic interactions in the gas phase, respectively. The solvation free energy ($\Delta G_{solv}$) is again separated into two segments:

$$\Delta \textbf{\textit{G}}_{\textbf{solv}} = \Delta \textbf{\textit{G}}_{\textbf{pol}} + \Delta \textbf{\textit{G}}_{\textbf{nonpol}} \quad \dots\dots\dots\dots\dots\dots\dots\dots\dots\dots\dots\dots\dots\dots\dots\dots\dots\dots\dots \text{[6]}$$

Where $\Delta G_{pol}$ and $\Delta G_{nonpol}$ are the polar and non-polar supplements to the solvation free energy, separately. The $\Delta G_{solv}$ is estimated with the PBSA component of AMBER set of program. The dielectric constant was fixed to 1.0 and 80.0 for the solute and solvent, respectively. The nonpolar

input of the solvation free energy is estimated as a function of the solvent-accessible surface area (SAS), as follows:

$$\Delta G_{nonpol} = (SAS) + \beta$$ …………………………………………………………………… [7]

where SAS was calculated by the MSMS software package, with 1.4 Å solvent probe radius. The empirical constant values for γ and β were set to 0.00542 kcal/mol, and 0.92 kcal/mol, respectively. Entropy effects ($-T\Delta S$) to the binding free energy comes from alterations of the translational, rotational and vibrational degrees of freedom, as follows:

$$\Delta S = \Delta S_{translational} + \Delta S_{rotational} + \Delta S_{vibrational}$$ …………………………………………......... [8]

$T\Delta S$ is usually calculated by means of classical statistical thermodynamics and normal mode analysis. Owing to entropy estimations for larger systems being exceptionally time consuming, only 50 snapshots were chosen at an interim of 100 ps from the entire trajectories. Individual snapshots were minimized until the root-mean-square of the energy gradient was lower than $10^{-4}$ kcal/mol/Å$^2$ with a distance dependent dielectric function $4R_{ij}$ (the distance between two atoms).

## 2.5. Residue-ligand interaction decomposition calculations:

Owing to the massive demand of computational assets for GB calculations, the contacts amongst the ligands and individual SARS-CoV-2 M$^{pro}$ residue was calculated by MM-GBSA decomposition method in the *mm-pbsa* segment in AMBER18. The binding interaction of each inhibitor-residue duos contains four terms: van der Waals ($\Delta E_{vdw}$), electrostatic ($\Delta E_{ele}$), polar solvation, ($\Delta G_{pol}$) and non-polar solvation ($\Delta G_{nonpol}$) contribution.

$$\Delta G_{inhibitor-residue} = \Delta E_{vdw} + \Delta E_{ele} + \Delta G_{pol} + \Delta G_{nonpol}$$ …………………………………………….[9]

The polar contribution ($\Delta G_{pol}$) to solvation energy was estimated by the GB (generalized-born) component and parameters for the GB calculation were established by the Amber team [Onufriev *et al*. 2000]. All energy components in Eq. (9) were estimated utilizing 500 snapshots from the entire 5.0 ns trajectories. PyMol package (www.pymol.org) was used for the graphic visualization and presentation of protein structures.

## 2.6. Hydrogen-bonds norms:

The stabilities of the SARS-CoV-2 M$^{pro}$ - inhibitor complexes were assessed by computing the hydrogen bonds (H-bonds) outlines utilizing the *hbond* tool of CPPTRAJ module [Roe and Cheatham III, 2013] in AmberTools19. The development of H-bonds described by a default distance cut-off of 3.0 Å and an angle cut-off 135°, between the donor and acceptor atoms. Percentage of occupancy were calculated by total number of H-bonds obtained by the total number of frames generated in the system which is multiplied by 100.

## 3. Results & Discussions:
### 3.1. Docking of the inhibitors against SARS-CoV-2 M$^{pro}$:

Molecular docking of the four inhibitors JE-2147, JE2-CH3, KNI-272 and KNI-227 were performed independently to the SARS-CoV-2 M$^{pro}$ and the inhibitors exhibited a binding energy of −8.0, −8.2, −7.8 and -7.6 kcal/mol, respectively. The docked inhibitors with the protease and the interacting residues in and adjoining active site region are shown in Figure 3. The conventional hydrogen bonding, carbon-hydrogen bonding and hydrophobic interactions between SARS-CoV-2 M$^{pro}$ and the four inhibitors docked are presented in Table-1.

**Table 1**: Inhibitors (JE-2147, JE2-CH3, KNI-227 and KNI-272) interacting with the residues from the active site and adjoining areas along with their binding energies from docking studies. The active site amino acids are specified in bold black.

| Sl. No. | Name of the protease inhibitors | Chemical Formula | PubChem CID: | Binding affinity (kcal/mol) | Amino acid residues Interacting with inhibitors |
|---|---|---|---|---|---|
| 1 | JE-2147 (Kynostatin-764) | $C_{32}H_{37}N_3O_5S$ | 446837 | -8.0 | Thr26, Leu27, **His41**, Met49, Asn142, **Cys145**, His164, Met165, Glu166, Pro168 |
| 2 | JE-2147-CH3 | $C_{33}H_{40}N_3O_5S$ | N/A | -8.2 | Thr26, **His41**, Met49, His41, Asn142, Met165, Glu166, Pro168, Thr190, Ala191 |
| 3 | KNI-272 (Kynostatin-272) | $C_{33}H_{41}N_5O_6S_2$ | 60927 | -7.8 | Leu27, **His41**, Met49, Asn142, **Cys145**, His163, Met165, Glu166, His172, Thr190 |
| 4 | KNI-227 (Kynostatin-227) | $C_{35}H_{45}N_5O_6S_2$ | 65012 | -7.6 | Thr26, Ser46, **His41**, Met49, Gly143, Met165, Glu166 |
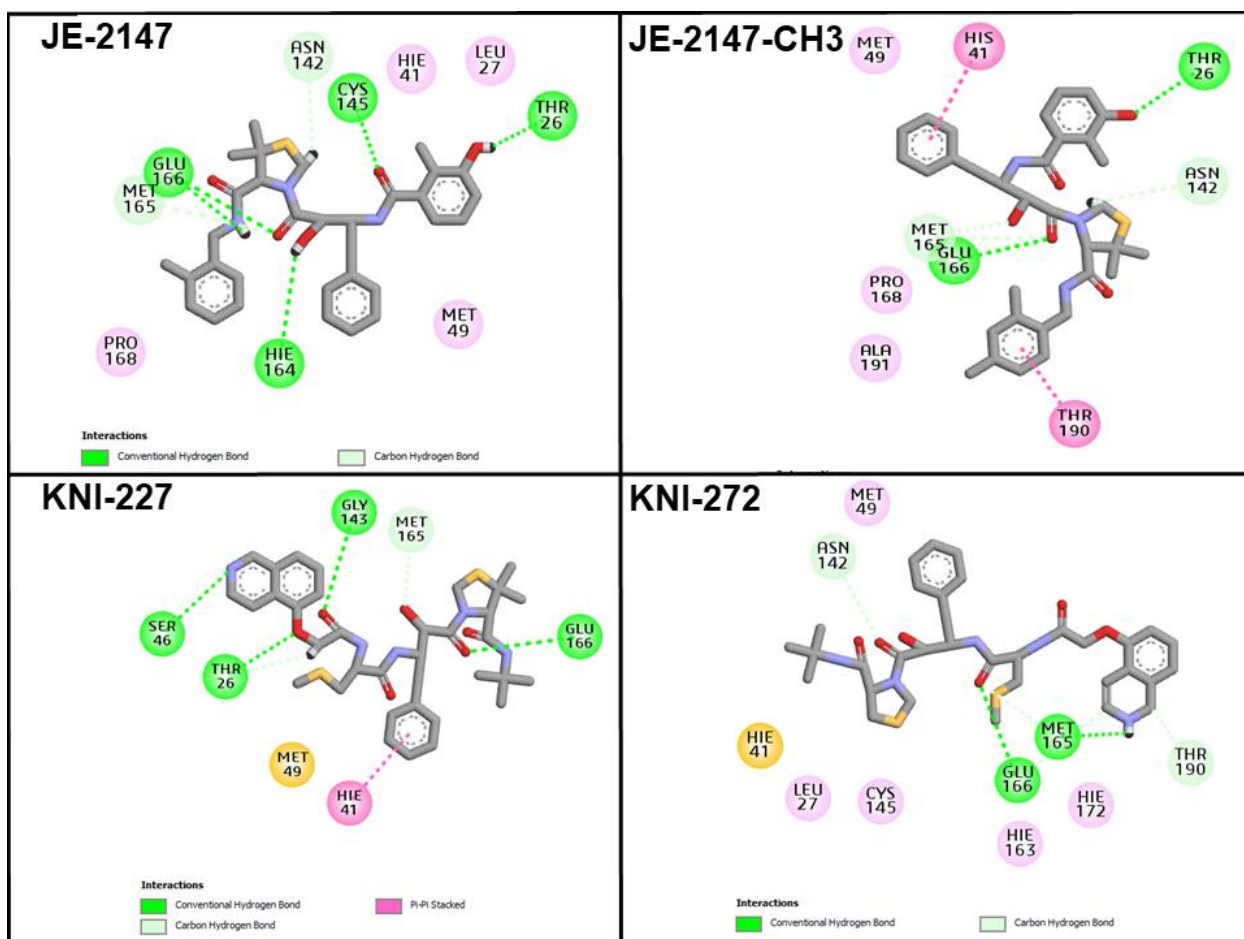
**Figure 3:** Particulars of numerous types of interactions exists between the amino acids nearby the active site of SARS-CoV-2 M^pro for all the four APNS containing inhibitors (JE-2147, JE2-CH3, KNI-227 and KNI-272). Ligands/inhibitors are shown in grey stick model and residues of interactions are shown in colored spheres. Green spheres: Conventional H-Bonds; Cyan spheres: Carbon Hydrogen bonds; Purple spheres: Pi-Pi stacked; Yellow spheres: Pi-Sulfur.

## 3.2. Conformational stability and compactness analysis:

To study the variation in the protein dynamics and the conformational stability of the protein-ligand complex, the protein complexed with four inhibitors were subjected to 5.0 ns MD simulations and the root-mean square deviation (RMSD) of the Cα atoms were calculated relative to the starting conformations and presented in Figure 4. The RMSD plots shows that the conformations of the SARS-CoV-2 complexed with JE-2147, JE2-CH3, KNI-227 and KNI-272 are in good equilibrium and stability is maintained throughout due to their lower RMSD. The entire four protein-ligand complex trajectories go parallel to each other until the end of the simulations ranging between 0.5 Å to a maximum of 2.5 Å. The trajectory for M^pro-KNI227 fluctuates a bit

more after 3 ns jumping to as high as 2.5 Å, however eventually it comes down to go parallel with others. The average RMSD values of trajectories for JE-2147, JE2-CH3, KNI-272 and KNI-227 were found to be 1.35, 1.39, 1.23, and 1.61 Å, respectively with corresponding standard deviations (SD) of 0.16, 0.17, 0.18, and 0.41 Å.
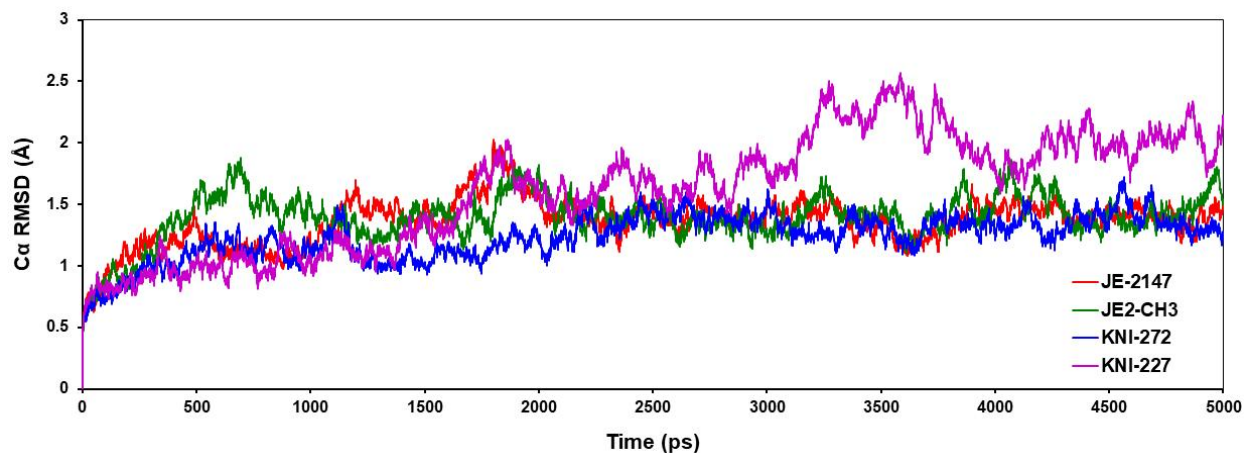


**Figure 4**. RMSD plot for backbone Cα atoms relative to their initial minimized complex structures (SARS-CoV-2 M$^{pro}$ + inhibitors) as a function of time.

The structural compactness of individual system was investigated by valuing the radius of gyration (R$_g$) from their corresponding simulation trajectories, and the estimated average values are described in Figure S1 and Table T1. An analogous R$_g$ is achieved for all the systems except for JE2-CH3, where the average Rg value is 22.31 with SD of 0.18, suggesting a relatively higher flexibility and less compactness as compared to the other three systems.

## 3.3. Conformational flexibility analysis from RMSF:

With the aim of analyzing the detailed residual atomic fluctuations, the root mean square fluctuations (RMSF) of the Cα atoms have been accomplished for the protease-inhibitor complexed structures as illustrated in Figure 5. RMSF values of the SARS-CoV-2 M$^{pro}$ structure confirmed that the binding site residues (His41 and Cys145) exhibited less fluctuations. The average RMSF values were 0.43, 0.41, 0.39, and 1.29 Å for JE-2147, JE2-CH3, KNI-272 and KNI-227, respectively, suggesting a higher rate of conformational fluctuations in the protease complex with KNI-227 as compared to others three.
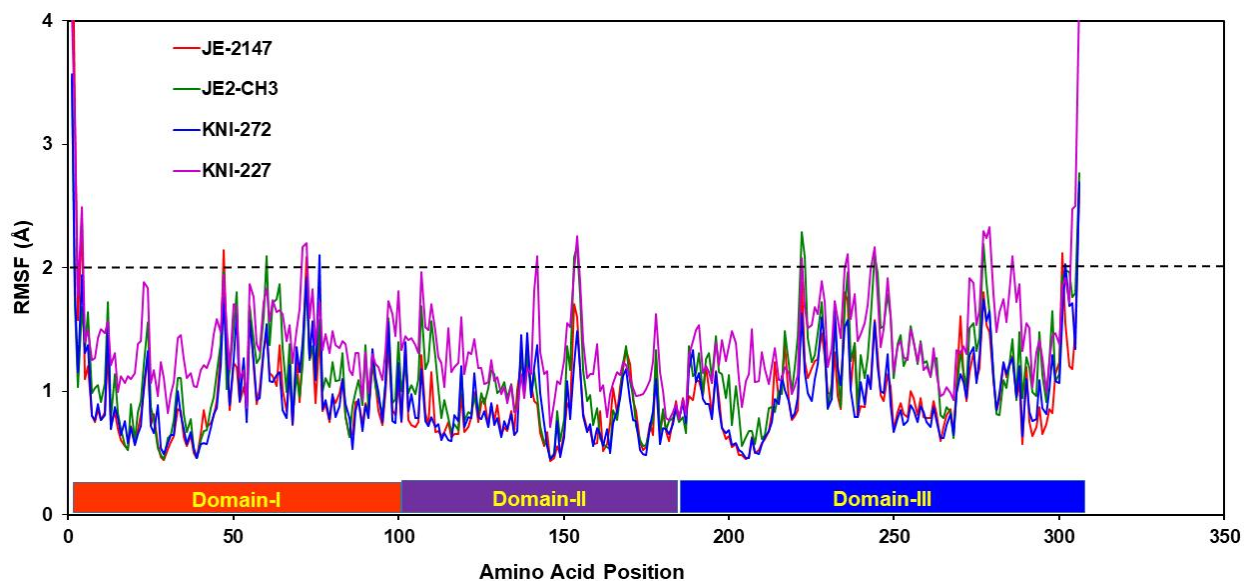
**Figure 5**: RMSF of Cα atoms vs. residue number of the inhibitors complexed SARS-CoV-2 M$^{pro}$ structure. Residues with higher fluctuations and larger than 2.0 Å are labelled by a cutoff dashed line.


## 3.4. Binding Free Energy analysis:

To get insights to the binding affinity of the four inhibitors JE-2147, JE2-CH3, KNI-227 and KNI-272 to SARS-CoV-2 M$^{pro}$ structure, absolute binding free energies were estimated for all the complexes by MM-GBSA scheme. Contributions of the binding free energies of JE-2147, JE2-CH3, KNI-227 and KNI-272 bound complexes are briefed in Table 2 and Figure 6. As displayed in the figure and table, the calculated binding free energies ($\Delta G_{Total}$) of four inhibitors were -54.66, -46.41, -51.82 and –44.98 kcal/mole, respectively. This suggests that binding free energy of all four (JE-2147, JE2-CH3, KNI-227 and KNI-272) complexes are reasonably higher than the binding affinities of the other HIV-protease inhibitors Indinavir (-17.23 kcal/mol), Darunavir (-22.78 kcal/mol) [Sang *et al*.,2020], and Lopinavir (-30.56 kcal/mol) [Wang *et al*.2020] reported earlier.
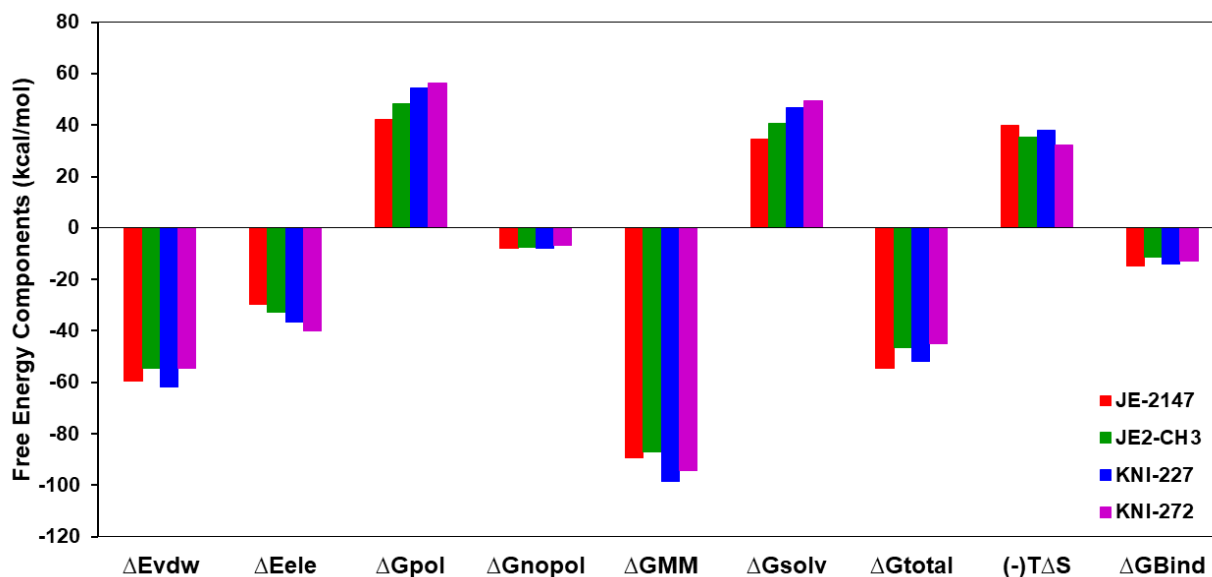
**Figure 6**: Energy components (kcal/mol) for the binding of inhibitors to the SARS-CoV-2 M$^{pro}$. $\Delta E_{vdw}$, van der Waals energy; $\Delta E_{elec}$, electrostatics energy in the gas phase; $\Delta G_{pol}$, polar solvation energy; $\Delta G_{nonpol}$, nonpolar solvation energy; $T\Delta S$, overall entropy contribution and $\Delta G_{Total}$, total binding energy. $\Delta G_{Bind} = \Delta G_{total} - T\Delta S$.

In accord with the components of the binding free energy from Table 2, in all the four SARS-CoV-2 M$^{pro}$/Ligand complexes, van der Waals and electrostatic energies in the gas phase offer the key favorable contributions to the inhibitor binding. Non-polar solvation energies ($\Delta G_{nonpol}$), arose from the burial of ligand's solvent accessible surface area (SASA), has also influences to the binding energy in a favorable way. On the contrary, polar solvation energies ($\Delta G_{pol}$) and entropy components ($-T\Delta S$) generate substantial unfavorable contribution to the binding energy. Additionally, Table-2 depicts that the calculated binding free energy ($\Delta G_{Total}$) of JE-2147 is greater (-54.66 kcal/mol) than JE2-CH3 (-46.41 kcal/mol), KNI-272 (-51.82 kcal/mol) and KNI-227 (-44.98 kcal/mol) suggesting that JE-2147 is more effective against SARS-CoV-2 M$^{pro}$ compared to the three other inhibitors studied.

**Table 2**: Binding free energy components for the SARS-CoV-2 M$^{pro}$/Ligand complex calculated from 500 snapshots (extracted from 1$^{st}$–5$^{th}$ ns) through MM-GBSA.[a]

| | MM-GBSA Calculation | | | | | | | | | | |
|---|---|---|---|---|---|---|---|---|---|---|---|
| | JE-2147 | | JE-2147-CH3 | | KNI-227 | | KNI-272 | | IND[h] | DAR[h] | LOP[i] |
| Components[b] | Mean | Std[g] | Mean | Std[g] | Mean | Std[g] | Mean | Std[g] | Mean | Mean | Mean |
| $\Delta E_{vdw}$ | -59.64 | 4.19 | -54.53 | 4.69 | -61.93 | 4.49 | -54.39 | 3.09 | -41.00 | -41.27 | -20.09 |
| $\Delta E_{ele}$ | -29.51 | 7.32 | -32.67 | 7.57 | -36.62 | 7.77 | -40.03 | 9.35 | -13.14 | -5.79 | -52.46 |
| $\Delta G_{pol}$ | 42.24 | 5.53 | 48.31 | 6.22 | 54.56 | 7.30 | 56.33 | 7.69 | 41.48 | 28.98 | 46.58 |
| $\Delta G_{nonpol}$ | -7.75 | 0.32 | -7.52 | 0.57 | -7.83 | 0.56 | -6.88 | 0.37 | -4.57 | -4.74 | -4.59 |
| $\Delta E_{MM}$ [c] | -89.15 | 7.46 | -87.21 | 8.91 | -98.56 | 10.22 | -94.43 | 9.81 | -54.14 | -47.06 | -30.56 |
| $\Delta G_{solv}$ [d] | 34.49 | 5.51 | 40.79 | 5.97 | 46.73 | 6.85 | 49.44 | 7.42 | 36.90 | 24.23 | 41.99 |
| $\Delta G_{total}$ [e] | **-54.66** | 4.66 | **-46.41** | 5.56 | **-51.82** | 4.84 | **-44.98** | 4.44 | **-17.23** | **-22.78** | **-30.56** |
| $-T\Delta S$ [f] | 39.71 | | 35.22 | | 37.89 | | 32.14 | | N/A | N/A | 23.93 |
| $\Delta G_{(Bind)}$ | **-14.95** | | **-11.19** | | **-13.93** | | **-12.84** | | N/A | N/A | **-6.63** |

[a] All values are given in kcal/mol.
[b] Components: E$_{vdw}$, van der Waals energy; E$_{ele}$, electrostatic energy in the gas phase; G$_{nonpol}$, non-polar solvation energy; $\Delta$G$_{pol}$, polar solvation energy.

[c] $\Delta E_{MM} = \Delta Evd_W + \Delta E_{ele}$, [d] $\Delta G_{solv} = \Delta G_{nonpol} + \Delta G_{pol}$, [e] $\Delta G_{total} = E_{vdW} + \Delta E_{ele} + \Delta G_{nopol} + \Delta G_{pol}$, [f] $\Delta S$= total entropy contribution, $\Delta G_{Bind} = E_{vdw} + \Delta E_{ele} + \Delta G_{nonpol} + \Delta G_{pol} - (T\Delta S)$
[g] Standard deviations (Std).
[h] IND: Indinavir, DAR: Darunavir (Data obtained from the reference: [Sang *et. al.* 2020])
[i] LOP: Lopinavir (Data obtained from the reference: [Wang *et. al.* 2020])

Subsequently, the binding affinity of all the four inhibitors was further estimated and matched with the FDA (Food and Drug Administration) permitted HIV-protease inhibitors, like lopinavir, indinavir and darunavir, which have been testified as effective drugs against SARS-CoV-2 M$^{pro}$. In recent times, the molecular contacts of lopinavir by the SARS-CoV-2 M$^{pro}$ has been explored using the MM-PBSA methodology [Wang 2020], and the binding free energy ($\Delta G_{Bind}$) of lopinavir was observed to be smaller (-06.63 kcal/mol) than JE-2147 (-14.95), JE2-CH3 (-11.19), KNI-227 (-13.93) and KNI-272 (-12.84) kcal/mol (check Table-2). It is further shown that for the complex formation, the electrostatic interaction (-52.46 kcal/mol) preferred more compared to the van der Waals interactions (-20.09 kcal/mol) in case of lopinavir. This is in contradiction to that has been witnessed for all the four inhibitors studied. In the case of all the four inhibitors, the van der Waals interactions ($\Delta E_{vdw}$) is more favorable as compared to the intermolecular electrostatic interactions

($\Delta E_{ele}$). Likewise, for instance in darunavir and indinavir, the van der Waals energy is more favorable (-41.27 & -41.00 kcal/mol, respectively) than the electrostatic energy (-5.79 and -13.14 kcal/mol) [Sang *et al*. 2020]. The current learning accounts that the binding affinity falls in the resulting order against SARS-CoV-2 M$^{pro}$: JE-2147 > KNI-227 > KNI-272 > JE2-CH3 > Lopinavir > Indinavir > Darunavir (check Table 2). Hence, the HIV-protease inhibitors containing the APNS, could be reflected as lead compounds in the finding of rational drugs against SARS-CoV-2 M$^{pro}$.

To understand and to explore the hotspot residues involved in the binding process in the complexes, the analysis of structure-activity relationship has been accomplished by carrying out the per-residue decomposition of free energy using MM-PBSA. The binding free energy was decomposed into inhibitor–residue sets to form an inhibitor–residue interaction scale as displayed in Figure 7a–d. A hotspot residue is considered, when it has more than -1.0 kcal/mol of interaction energy and is labelled in Table 3.
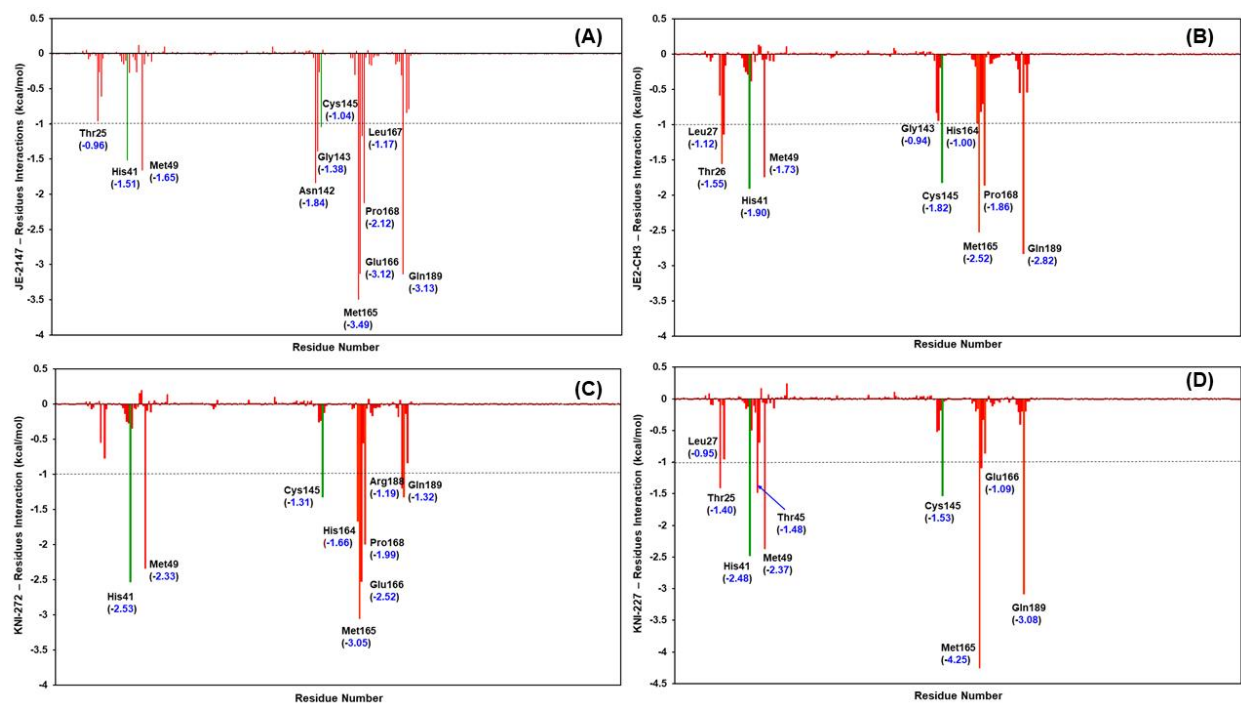


**Figure 7**: Decomposition of $\Delta G$ on a per-residue basis for the SARS-CoV-2 M$^{pro}$ - inhibitor complex: (a) JE-2147, (b) JE2-CH3, (c) KNI-272 and (d) KNI-227.

**Table 3**: Residue decomposition of $\Delta G_{total}$ on a per-residue basis (GB). [a]

| Residue | $E_{vdw}$ | $E_{ele}$ | $G_{pol}$ | $G_{nonpol}$ | $G_{side\_chain}$ | $G_{backbone}$ | $G_{Total}$ |
|---|---|---|---|---|---|---|---|
| **MM-GBSA Calculations** | | | | | | | |
| **SARS-CoV-2 M$^{pro}$ – JE-2147** | | | | | | | |
| Met165 | -2.403 | -2.000 | 1.120 | -0.215 | -1.874 | -1.623 | -3.497 |
| Gln189 | -3.490 | -2.016 | 2.964 | -0.593 | -2.871 | -0.265 | -3.136 |
| Glu166 | -2.540 | -2.209 | 2.028 | -0.405 | -0.777 | -2.349 | -3.126 |
| Pro168 | -1.828 | -0.038 | 0.094 | -0.353 | -1.629 | -0.496 | -2.125 |
| Asn142 | -2.328 | -2.182 | 3.116 | -0.447 | -0.729 | -1.112 | -1.841 |
| Met49 | -1.535 | -0.036 | 0.065 | -0.150 | -1.391 | -0.266 | -1.657 |
| His41 | -1.855 | -0.971 | 1.437 | -0.128 | -1.351 | -0.167 | -1.518 |
| Gly143 | -0.622 | -2.228 | 1.587 | -0.124 | -0.259 | -1.128 | -1.387 |
| Leu167 | -1.555 | 0.167 | 0.244 | -0.029 | -0.755 | -0.418 | -1.173 |
| Cys145 | -0.899 | -0.239 | 0.221 | -0.124 | -0.717 | -0.323 | -1.040 |
| Thr25 | -0.548 | -0.300 | -0.015 | -0.093 | -0.453 | -0.505 | -0.958 |
| **SARS-CoV-2 M$^{pro}$ – JE2-CH3** | | | | | | | |
| Thr26 | 0.278 | -4.469 | 2.757 | -0.121 | 0.002 | -1.557 | -1.555 |
| Leu27 | -0.731 | -0.404 | 0.047 | -0.041 | -0.731 | -0.399 | -1.129 |
| His41 | -1.928 | -0.573 | 0.744 | -0.144 | -1.565 | -0.336 | -1.901 |
| Met49 | -1.775 | -0.034 | 0.312 | -0.240 | -1.373 | -0.365 | -1.738 |
| Cys145 | -1.356 | -0.273 | -0.017 | -0.173 | -1.481 | -0.339 | -1.820 |
| Met165 | -2.030 | -1.390 | 1.116 | -0.219 | -1.651 | -0.872 | -2.523 |
| Pro168 | -1.689 | -0.208 | 0.367 | -0.331 | -1.542 | -0.319 | -1.861 |
| Gln189 | -2.462 | -4.993 | 5.190 | -0.563 | -2.550 | -0.278 | -2.828 |
| | | | | | | | |
| **SARS-CoV-2 M$^{pro}$ – KNI-272** | | | | | | | |
| Met165 | -1.843 | -1.477 | 0.450 | -0.183 | -1.294 | -1.759 | -3.053 |
| His41 | -2.386 | -0.680 | 0.694 | -0.160 | -2.200 | -0.333 | -2.533 |
| Glu166 | -1.734 | -6.261 | 5.839 | -0.367 | -0.511 | -2.012 | -2.523 |
| Met49 | -2.298 | -0.767 | 0.997 | -0.265 | -2.281 | -0.054 | -2.335 |
| Pro168 | -1.830 | -0.340 | 0.476 | -0.296 | -1.358 | -0.633 | -1.991 |
| His164 | -0.593 | -4.148 | 3.148 | -0.070 | -0.193 | -1.471 | -1.664 |
| Gln189 | -2.865 | -0.798 | 2.855 | -0.513 | -1.022 | -0.299 | -1.321 |
| Cys145 | -1.225 | -0.063 | 0.110 | -0.140 | -1.109 | -0.209 | -1.318 |
| Arg188 | -1.271 | 0.961 | -0.801 | -0.080 | -0.042 | -1.149 | -1.191 |
| **SARS-CoV-2 M$^{pro}$ – KNI-227** | | | | | | | |
| Met165 | -2.574 | -2.392 | 0.970 | -0.256 | -2.254 | -1.997 | -4.252 |
| Gln189 | -2.704 | -6.170 | 6.374 | -0.579 | -3.021 | -0.058 | -3.079 |
| His41 | -2.148 | -1.098 | 0.916 | -0.149 | -2.203 | -0.276 | -2.479 |
| Met49 | -2.305 | -0.585 | 0.818 | -0.299 | -2.200 | -0.171 | -2.371 |
| Cys145 | -1.179 | -0.743 | 0.569 | -0.179 | -1.376 | -0.157 | -1.533 |
| Thr45 | -0.803 | -1.317 | 0.665 | -0.026 | -0.160 | -1.323 | -1.482 |
| Thr25 | -1.451 | -0.180 | 0.435 | -0.212 | -0.930 | -0.477 | -1.407 |
| Glu166 | -1.970 | -2.596 | 3.861 | -0.385 | -0.833 | -0.257 | -1.090 |
| Leu27 | -0.996 | 0.088 | 0.039 | -0.084 | -0.954 | 0.001 | -0.953 |

Figure 7a–d demonstrates that, the overall outlines in the interaction spectra of four SARS-CoV-2 M$^{pro}$/ligand complexes are analogous, though there is a variance in discrete residue interaction spectrum. Overall, the key interactions arise from a group of hotspot residues like Leu27, His41, Met49, Cys145, His164, Met165, Glu166, Leu167, Pro168, and Gln189, which contributes favorably to the binding event. Moreover, it can be observed that the catalytic residue, His41 and Cys145 also contribute sensibly (> 1.0 kcal) to the binding of the four inhibitors to the protease. Nevertheless, the unfavorable polar solvation energies negate the net binding energies owing to their solvation in aqueous solution. Residues like Ser46, Glu47 have relatively unfavorable polar solvation energies with ≥0.2 kcal/mol.

## 3.5. Hydrogen bonds (H-bonds) analysis:

In order to compliment the binding affinities of the inhibitors, the binding stabilities in all the four complexes with SARS-CoV-2 M$^{pro}$ structure were examined during the 5.0 ns MD simulations trajectory period and the H-bonds occupancy are described in Table-4 and the number of H-bonds as a function of time is presented in Figure 8. From Figure 8, it was observed that, the protein-ligand complex of KNI-272 with SARS-CoV-2 M$^{pro}$ structure has the maximum (2.33) average number of H-bonds per time frame during the simulation phase. The average numbers of H-bonds witnessed for KNI-227, JE2-CH3, and JE-2147 were 2.24, 2.21 and 2.02, respectively. The analysis revealed that, at least two hydrogen bonds are always present between the protease and the inhibitors, throughout the simulation period, suggesting a tight interactions of the inhibitors to the protease active site region.

From Table-4, it was observed that in the case of M$^{pro}$/JE-2147, residues like Glu166 (70.86%, 51.84%), and Gly143 (41.26%) make H-bonds with the inhibitor with an occupancy of at least 40% throughout the simulation time. Conversely, for instance in M$^{pro}$/JE2-CH3 complex, the maximum H-bonds occupancy is acquired for by Thr26 (91.20 %) along with two other residues His164 and Gln189 contributing 59.06 % and 51.46 %, respectively. Apart from that, the active site residue His41 also contributes marginally by 7.12% to the bonding throughout the simulation time. Furthermore, in the case of M$^{pro}$/KNI-272, at least two residues: His164 and Glu166 contributes 75.04 % and (70.46% for Glu166@N, 52.46 % for Glu166@N), respectively. Finally, in the case of M$^{pro}$/KNI-227 also, two residues like Glu166 and Gln189 contributes significantly by 87.96 % (from Glu166@N) and 62.14 % (Gln189@NE2) & 53.24 % (Gln189@OE1). From

these observations (from Table-4 and Figure-8), we found that the H-bonding patterns in case of all the protease/ligand complexes is managed by formation of at least two H-bonds throughout and with an occupancy of at least 40% of the simulation frames.

**Table 4**: Hydrogen bonds present between SARS-CoV-2 M$^{pro}$ and the inhibitors with the respective average distances, average angles and percentage of occupancy in the MD simulations trajectories. H-bonds with an occupancy of at least 5.0 % are listed in table and >40% are depicted in bold.

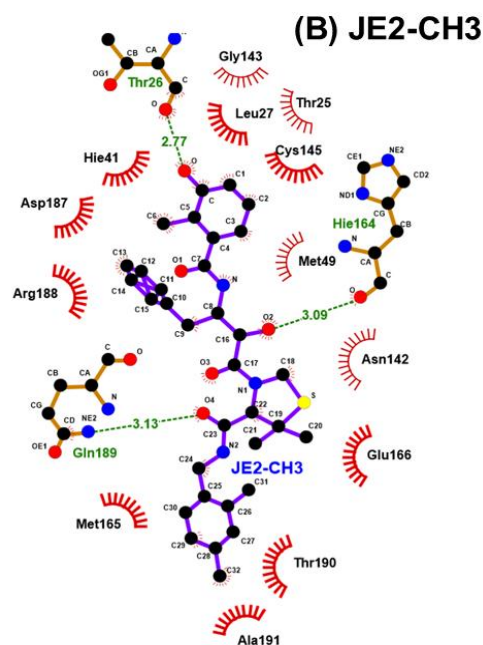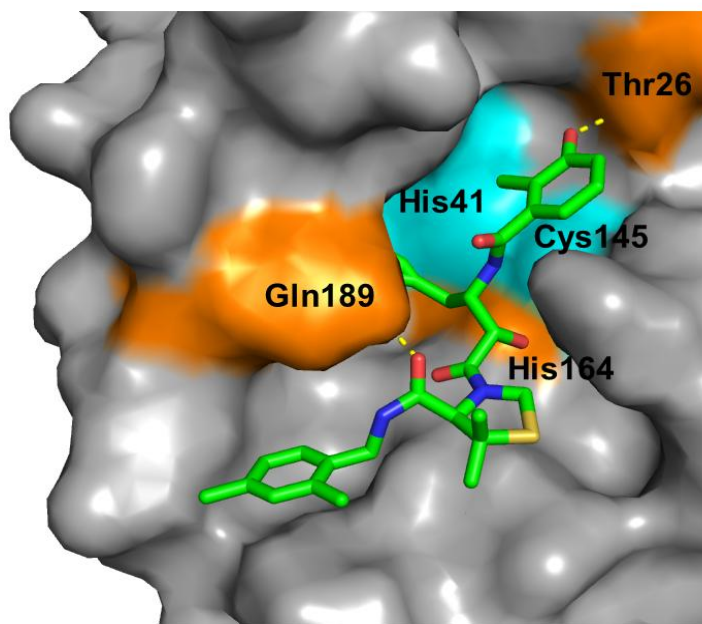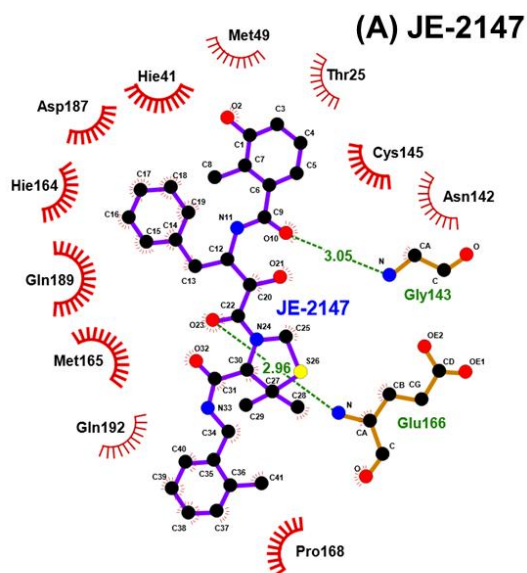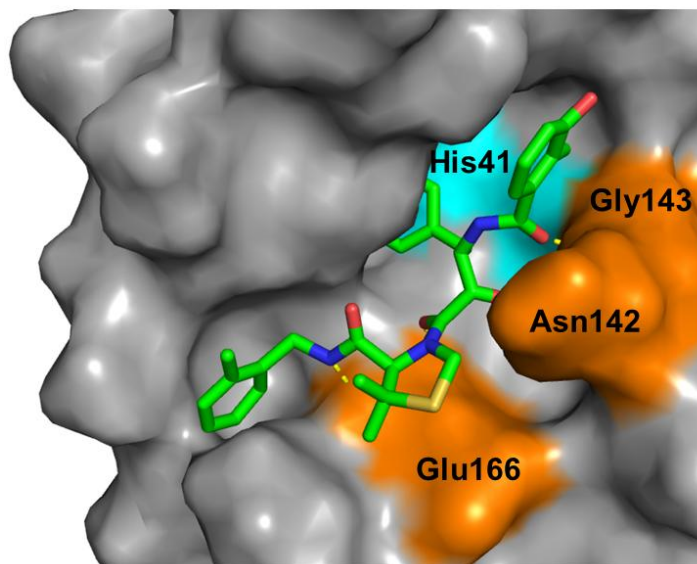| | Binding pairs | | MD | | | |
|---|---|---|---|---|---|---|
| | Acceptor atom | Donor atom | Avg. Distance (Å) | Avg. Angle (°) | Frames (n) | Occupancy (%) |
| SARS-CoV-2 M$^{pro}$ – JE-2147 | | | | | |
| 1 | Glu166@O | JE-2147@N33 | 2.8462 | 156.4306 | 3543 | **70.86** |
| 2 | JE-2147@O23 | Glu166@N | 2.8820 | 159.3427 | 2592 | **51.84** |
| 3 | JE-2147@O10 | Gly143@N | 2.8814 | 160.7390 | 2063 | **41.26** |
| 4 | Thr26@O | JE-2147@O2 | 2.7612 | 147.5246 | 592 | 11.84 |
| 5 | JE-2147@O32 | Gln189@NE2 | 2.8339 | 162.0320 | 450 | 9.00 |
| 6 | JE-2147@O2 | Thr26@N | 2.9195 | 158.0250 | 259 | 5.18 |
| | | | | | | |
| SARS-CoV-2 M$^{pro}$ – JE2-CH3 | | | | | |
| 1 | Thr26@O | JE2-CH3@O | 2.7265 | 163.1755 | 4560 | **91.20** |
| 2 | His164@O | JE2-CH3@O2 | 2.7940 | 153.4040 | 2953 | **59.06** |
| 3 | JE2-CH3@O4 | Gln189@NE2 | 2.8578 | 159.9289 | 2573 | **51.46** |
| 4 | His41@ND1 | JE2-CH3@O | 2.8762 | 152.1498 | 356 | 7.12 |
| 5 | Gln189@OE1 | JE2-CH3@N2 | 2.8902 | 159.3999 | 325 | 6.50 |
| 6 | JE2-CH3@O3 | Glu166@N | 2.9103 | 160.6712 | 301 | 6.02 |
| | | | | | | |
| SARS-CoV-2 M$^{pro}$ – KNI-272 | | | | | |
| 1 | His164@O | KNI-272@O2 | 2.7372 | 163.5501 | 3752 | **75.04** |
| 2 | KNI-272@O6 | Glu166@N | 2.8563 | 162.4502 | 3523 | **70.46** |
| 3 | Glu166@O | KNI-272@N2 | 2.8753 | 158.7376 | 2623 | **52.46** |
| 4 | KNI-272@O5 | Ser46@OG | 2.7341 | 162.6452 | 1476 | 29.52 |
| | | | | | | |
| SARS-CoV-2 M$^{pro}$ – KNI-227 | | | | | |
| 1 | KNI-227@O3 | Glu166@N | 2.8341 | 163.0258 | 4398 | **87.96** |
| 2 | KNI-227@O1 | Gln189@NE2 | 2.8561 | 161.4252 | 3107 | **62.14** |
| 3 | Gln189@OE1 | KNI-227@N2 | 2.8823 | 163.6643 | 2662 | **53.24** |
| 4 | KNI-227@O5 | Gly143@N | 2.8576 | 152.2745 | 647 | 12.94 |
| 5 | His164@O | KNI-227@O2 | 2.8164 | 149.3620 | 356 | 7.12 |
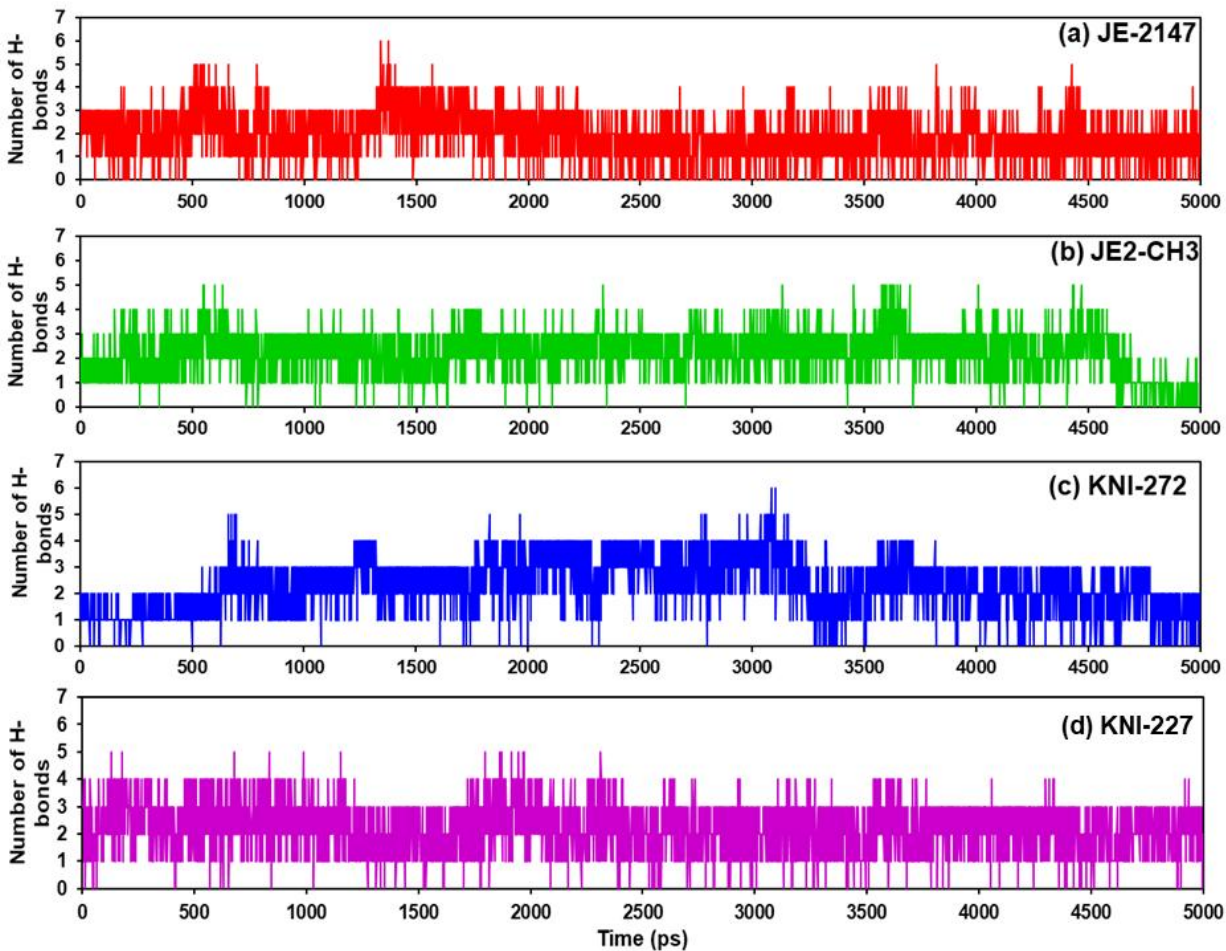
**Figure 8**: Average intermolecular Hydrogen-bonding number and variations in SARS-CoV-2 M$^{pro}$ – inhibitors (a) JE-2147, (b) JE2-CH3, (c) KNI-272 and (d) KNI-227) complexes during 5.0 ns MD simulations.

A comprehensive interaction outline of residues concerning H-bonds and hydrophobic interactions was also calculated by LigPlot+ software program (Laskowski & Swindells, 2011) and presented in Figure 9a-d. It recommends that many of the residues present in and around the active site region plays a noteworthy role in developing H-bonds with the inhibitors. Figure-9a, shows the interactions for the inhibitor JE-2147, where residues like Glu166 and Gly143 forms H-bonds with O23 and O10 of JE-2147, that can be confirmed from the Table-4. In the figure-9b, it can be seen that the inhibitor JE2-CH3 forms H-bonding with the residues like Thr26, His164 and Gln189 with the O, O2 and O4 atoms of JE2-CH3, respectively with more than 50% occupancy of the total frames in the simulation. For the interactions with KNI-272, as shown in Fig. 9c, residues like His164 and Glu166 contributes through H-bonding making contacts at O2, O6 and N2 atoms of

KNI-272. For KNI-227, as shown in Fig. 9d, residues like Glu166 and Gln189, plays the role in binding events through H-bonds making contacts at O3, O1 and N2 atoms of KNI-227. For all other interacting residues as shown in the Fig. 9a-d, including the catalytic dyad residues His41 and Cys145, has strong hydrophobic contacts with the inhibitors keeping them intact in the binding pocket. Overall, the H-bonds and hydrophobic interactions plays a significant role in the binding process.

**Figure 9**. Expected binding modes found from the MD simulation analyses of all the four inhibitors with the SARS-CoV-2 $M^{pro}$. Structures of SARS-CoV-2 $M^{pro}$ are shown as molecular surface model in grey. The inhibitor molecules are represented as stick model, and their contact residues in the protease are designed by LigPlot software package. His41 and Cys145, catalytic dyad residues are highlighted in cyan color. The hydrogen-bonds formed between inhibitors and $M^{pro}$ residues are labeled in orange for (A) SARS-CoV-2 $M^{pro}$-JE2147 complex. (B) SARS-CoV-2 $M^{pro}$ – JE2CH3 complex, (C) SARS-CoV-2 $M^{pro}$ – KNI272 complex and (D) SARS-CoV-2 $M^{pro}$ – KNI227 complex.

# 4. Conclusion:

We explored the mechanism of binding of four experimental HIV-protease inhibitors, viz. JE-2147, JE2-CH3, KNI-227 and KNI-272 to SARS-CoV-2 $M^{pro}$ by exhausting an all-atom MD simulation in ns time-scale in combination with the extensively practiced MM/PBSA method. In agreement with the energy components of the binding free energy, for all the four SARS-CoV-2 $M^{pro}$/inhibitor complexes the van der Waals ($E_{vdw}$) energies offer the foremost contributions to the inhibitor binding, along with intermolecular electrostatic interactions, and non-polar solvation free energy. We have also validated that the inhibitor JE-2147 is comparatively more effective than JE2-CH3, KNI-227 and KNI-272 thanks to an increased favorable input from the intermolecular van der Waals and decreased solvation energies. Comparison of the free energy estimations revealed that the APNS-based inhibitors be able to bind relatively higher than the potent anti-HIV drugs (Darunavir/Indinavir/Lopinavir). Free energy decomposition of residues and H-bonding indicated that, maximum of the residues that adds to the favorable binding of the inhibitors with the SARS-CoV-2 $M^{pro}$ come from the active site, and/or active site wall, suggesting these segments of the protease shows a significant role in binding event. Conclusively, our results point towards the importance of evolving drugs against COVID-19 using APNS-based inhibitors particularly like JE-2147. This is a very encouraging outcome interpreting the pre-testified antiviral roles of JE-2147. Accelerated experimental investigation in this direction is necessary by the widespread exploration of these APNS containing antiviral inhibitors against SARS-CoV-2 $M^{pro}$.

## Conflicts of Interest:
The authors declare that they have no conflict of interests.

# 5. References:

Abraham Peele, K., Chandrasai, P., Srihansa, T., Krupanidhi, T., Vijaya Sai, A., John Babu, D., Indira, M., Ranganadha A. R., Venkateswarulu. T.C., (2020) Molecular docking and dynamic simulations for antiviral compounds against SARS-CoV-2: A computational study. *Informatics in Medicine Unlocked*, 100345.

Baldwin ET, Bhat TN, Gulnik S, et al. (1995) Structure of HIV-1 protease with KNI-272, a tight-binding transition-state analog containing allophenylnorstatine. *Structure*, 3:581-590.

Bandyopadhyay, P. and Meher, B.R. (2006) Drug Resistance of HIV-1 protease against JE-2147: I47V mutation investigated by molecular dynamics simulation. *Chemical Biology & Drug Design.* 67: 155-161.

Bayly C.L., Cieplak P., Cornell W.D., Kollman P.A. (1993) A well-behaved electrostatic potential based method using charge restraints for determining atom-centered charges: the RESP model. *Journal of Physical Chemistry,* 97:1 0269.

Berendsen, H .J.C., Postma J.P.M., Van Gunsteren W.F., Dinola A., Haak J.R. (1984) Molecular dynamics with coupling to an external bath*. Journal of Chemical Physics*, 81:3684.

Case D.A. et al. (2018) AMBER 18. University of California, San Francis co, CA. USA.

Chen, Y., Yiu, C.-P., & Wong, K.-Y. (2020). Prediction of the SARS-CoV-2 (2019-nCoV) 3C-like protease (3CL pro) structure: Virtual screening reveals velpatasvir, ledipasvir, and other drug repurposing candidates. *F1000Research*, 9, 129.

Das, S., Sarmah, S., Lyndem, S., Roy, A.S. (2020) An investigation into the identification of potential inhibitors of SARS-CoV-2 main protease using molecular docking study. *Journal of Biomolecular Structure and Dynamics,* 0:1-11.

Dash, J. J., Purohit, P. and Meher, B.R. (2020) Binding Interactions of JE-2147 (Normal vs Methylated) to HIV-1 Protease: A Molecular Dynamics Simulation Study for Drug Design Strategy. *Proceedings of International Conference on Drug Discovery* (ICDD) 2020.

Dewar M.J.S., Zoebisch E.G., Healy E.F., Stewart J.P. (1985) Development and use of quantum mechanical molecular models. 76. AM1: a new general purpose quantum mechanical molecular model. *Journal of American Chemical Society*; 107:3902.

Elmezayen, A. D., Al-Obaidi, A., & Şahin, A. T. (2020). Drug repurposing for coronavirus (COVID-19): *in silico* screening of known drugs against coronavirus 3CL hydrolase and protease enzymes. *Journal of Biomolecular Structure and Dynamics*, 20: 1–12.

Enmozhi, S.K., Raja, K., Sebastine, I., Joseph, J. (2020) Andrographolide as a potential inhibitor of SARS-CoV-2 main protease: an in silico approach. *Journal of Biomolecular Structure and Dynamics* 0:1-7.

Essmann U., Perera L., Berkowitz M.L., Darden, T. Lee, H, Pedersen, L.G. (1995) A smooth particle mesh ewald method. *Journal of Chemical Physics,* 103 :8577.

Islam, R., Parves, M.R., Paul, A.S., Uddin, N., Rahman, M.S., Mamun, A.A., Hossain, MN, Ali, MA and Halim. M.A. (2020) A molecular modeling approach to identify effective antiviral phytochemicals against the main protease of SARS-CoV-2, *Journal of Biomolecular Structure and Dynamics*. 0:1-12.

Jorgensen W.L., Chandrasekhar J., Madura J.D. (1983) Comparison of simple potential functions for simulating liquid water. *Journal of Chemical Physics*; 79:926.

Joshi, R. S., Jagdale, S. S., Bansode, S. B., Shiva Shankar, S., Tellis, M. B., Pandya, V. K., Chugh, A., Giri, A.P., Kulkarni, M. J. (2020) Discovery of potential multi-target-directed ligands by targeting host-specific SARS-CoV-2 structurally conserved main protease. *Journal of Biomolecular Structure and Dynamics,* 0:1-16.

Kageyama, S. *et al.*, H. Mitsuya. (1993), In *vitro* anti-human immunodeficiency virus (HIV) activities of transition state mimetic HIV protease inhibitors containing allophenylnorstatine. *Antimicrobial Agents Chemotherapy*, 37: 810-817.

Khan, R. J., Jha, R. K., and Amera, G. M. (2020). Targeting SARS-CoV-2: A systematic drug repurosing approach to identify promising inhibitors against 3C-like proteinase and 2′-O-ribose methyltransferase. *Journal of Biomolecular Structure and Dynamics*, 20: 1–14.

Laskowski R.A., Swindells M.B. (2011) LigPlot+: multiple ligand-protein interaction diagrams for drug discovery. *Journal of Chemical Information & Modeling*., 51:2778-86.

Lim, K. P. ; Ng, L. F. P. and Liu, D. X. (**2000**) Identification of a novel cleavage activity of the first Papain-Like Proteinase domain encoded by Open Reading Frame 1a of the Coronavirus Avian Infectious Bronchitis Virus and characterization of the cleavage products. *Journal of Virology*. 74 : 1674-1685.

Lobo-Galo, N., Terrazas-López, M., Martínez-Martínez, A., Gabriel Díaz-Sánchez, A. (2020) FDA-approved thiol-reacting drugs that potentially bind into the SARS-CoV-2 main protease, essential for viral replication. *Journal of Biomolecular Structure and Dynamics* 0:1-9.

Lu I-L, Mahindroo N, Liang P-H, Peng Y-H, Kuo C-J, Tsai K-C, et al. (**2006**) Structure-based drug design and structural biology study of novel nonpeptide inhibitors of severe acute respiratory syndrome coronavirus main protease. *Journal of medicinal chemistry*. 49:5154-61.

Mahanta, S., Chowdhury, P., Gogoi, N., Goswami, N., Borah, D. Kumar, R., Chetia, D., Borah, P., Buragohain, A.K., Gogoi. B. (2020) Potential anti-viral activity of approved repurposed drug against main protease of SARS-CoV-2: an *in silico* based approach. *Journal of Biomolecular Structure and Dynamics*, 0:1-15.

Maier, J.A., Martinez, Kasavajhala, K., Wickstrom, L., Hauser K.E. and Simmerling. C. (2015) ff14SB: Improving the accuracy of protein side chain and backbone parameters from ff99SB. *Journal of Chemical Theory & Computation,* 11, 3696-3713.

Meher, B.R., and Wang, Y. (2012). Binding of Single walled carbon nanotube to WT and mutant HIV-1 proteases: Analysis of flap dynamics and binding mechanism. *Journal of Molecular Graphics and Modeling,* 38:430-445.

Meher, B.R., and Wang, Y. (2012). Interaction of I50V mutant and I50L/A71V double mutant to HIV-1 protease inhibitor TMC114 (Darunavir): Molecular Dynamics and Free energy studies. *Journal of Physical Chemistry B,* 116:1884-1900.


Meher, B.R., and Wang, Y. (2015). Exploring the drug resistance of V32I and M46L mutant HIV-1 protease to inhibitor TMC114: Flap Dynamics and binding free energy studies. *Journal of Molecular Graphics and Modeling,* 56: 60 -73.

Meher, B.R. Purohit, P. and Dash, J. J., (2020) Probing phytochemicals as prospective antiviral agents against HIV-1 Protease through structure-based Virtual Screening and Molecular Dynamics simulations. *Proceedings of International Conference on Drug Discovery* (ICDD) 2020.

Miller III, B.R., McGee Jr., T.D., Swails, J.M., Homeyer, N., Gohlke, H., and Roitberg, A.E. (2012) MMPBSA.py: An efficient program for end-state free energy calculations. *Journal of Chemical Theory & Computation*, 8: 3314-3321.

Morris, G. M., Huey, R., Lindstrom, W., Sanner, M. F., Belew, R. K., Goodsell, D. S. and Olson, A. J. (2009) Autodock4 and AutoDockTools4: automated docking with selective receptor flexibility. *Journal of Computational Chemistry,* 16: 2785-91.

Muralidharan, N., Sakthivel, R., Velmurugan, D., Michael Gromiha, M. (2020) Computational studies of drug repurposing and synergism of lopinavir, oseltamivir and ritonavir binding with SARS-CoV-2 protease against COVID-19. *Journal of Biomolecular Structure and Dynamics* 0:1-6.


Nukoolkarn V, Lee VS, Malaisree M, Aruksakulwong O, Hannongbua S. (2008) Molecular dynamic simulations analysis of ritronavir and lopinavir as SARS-CoV 3CLpro inhibitors. *Journal of theoretical biology*. 254 :861-867.


Onufriev, A., Bashford, D., Case, D.A. (2000) Modification of the generalized Born model suitable for macromolecules, *Journal of Physical Chemistry B*, 104: 3712–3720.

Purohit, P. Dash, J. J., and Meher, B.R. (2020) Exploration of phytocompounds as potential anti-Dengue agents against DENV NS2B/NS3 protease: Structure-based virtual screening and MD simulation studies. *Proceedings of International Conference on Drug Discovery* (ICDD) 2020.

Reddy AD, Suh SB, Ghaffari R, Singh NJ, Kim D-J, Han JH, et al. (**2003**) Bioinformatics analysis of SARS proteins and molecular dynamics simulated structure of an alpha-helix motif. *Bulletin-Korean Chemical Society*,24:899-900.


Roe, D.R., and Cheatham III, T.E., (2013) PTRAJ and CPPTRAJ: Software for processing and analysis of molecular dynamics trajectory data. *Journal of Chemical Theory & Computation*, 9: 3084-3095.

Ryckaert, J.P., Ciccotti, G., Berendsen, H.J.C. (1977) Numerical integration of the Cartesian equations of motion of a system with constraints: molecular dynamics of n-alkanes*, Journal of Computational Physics,* 23 :327–341.

Sang, P, Tian, SH, Meng, ZH, Yang, LQ (2020) Anti-HIV drug repurposing against SARS-CoV-2. *RSC Advances*, 10:15775–15783.


Sk, M.F., Roy, R., Jonniya, N.A., Poddar, S. and Kar, P. (2020) Elucidating biophysical basis of binding of inhibitors to SARS-CoV-2 main protease by using molecular dynamics simulations and free energy calculations. *Journal of Biomolecular Structure and Dynamics*, 0: 1-15.

Ton, A. T., Gentile, F., and Hsing, M. (2020). Rapid identification of potential inhibitors of SARS-CoV-2 main protease by deep docking of 1.3 billion compounds. *Molecular Informatics*, 39, 200002.
Trott, O. and Olson, A. J. (2010) AutoDock Vina: improving the speed and accuracy of docking with a new scoring function, efficient optimization and multithreading. *Journal of Computational Chemistry,* 31: 455-461.

Umesh, Kundu, D., Selvaraj, C., Singh, S.K., Dubey, V.K. (2020) Identification of new anti-nCoV drug chemical compounds from Indian spices exploiting SARS-CoV-2 main protease as target. *Journal of Biomolecular Structure and Dynamics* 0: 1-7.

Wahedi, H.M., Ahmad, S. and Abbasi, S.W. (2020) Stilbene-based natural compounds as promising drug candidates against COVID-19. *Journal of Biomolecular Structure and Dynamics,* 0: 1-11.

Wang, J. (2020) Fast Identification of Possible Drug Treatment of Coronavirus Disease-19 (COVID-19) Through Computational Drug Repurposing Study. *Journal of Chemical Information & Modeling,* 0: 0-0.

Wang, J., Wolf, R.M., Caldwell, J.W., Kollman, P.A., Case, D.A. (2004) Development and testing of a general amber force field, *Journal of Computational Chemistry.* 25 1157–1174.

WHO (World Health Organization) www.who.int/dg/speeches/detail

Wu, F., S. Zhao, B. Yu, Y.-M. Chen, W. Wang, Z.-G. Song, Y. Hu, Z.-W. Tao, J.-H. Tian, Y.-Y. Pei, M.-L. Yuan, Y.-L. Zhang, F.-H. Dai, Y. Liu, Q.-M. Wang, J.-J. Zheng, L. Xu, E. C. Holmes, Y.-Z. Zhang, (**2020**) A new coronavirus associated with human respiratory disease in China. *Nature,* 579: 265–269.

Xia B, Kang X. (**2011**) Activation and maturation of SARS-CoV main protease. *Protein & cell*.;2:282-90.

Yamamoto N, Yang R, Yoshinaka Y, Amari S, Nakano T, Cinatl J, et al. (2004) HIV protease inhibitor nelfinavir inhibits replication of SARS-associated coronavirus. *Biochemical and biophysical research communications*. 318:719-25.

Yoshimura, K., Ryohei Kato, Keisuke Yusa, Mark F. Kavlick, Victor Maroun, Aline Nguyen, Tsutomu Mimoto, Takamasa Ueno, Makoto Shintani, Judith Falloon, Henry Masur, Hideya Hayashi, John Erickson, Hiroaki Mitsuya. (1999) JE-2147: A dipeptide protease inhibitor (PI) that potently inhibits multi-PI-resistant HIV-1. *PNAS*, 96: 8675-8680.

Zhang XW, Yap YL. (2004) Old drugs as lead compounds for a new disease? Binding analysis of SARS coronavirus main proteinase with HIV, psychotic and parasite drugs. *Bioorganic & medicinal chemistry*. 12:2517-2521.

Zhou, P. X.-L. Yang, X.-G. Wang, B. Hu, L. Zhang, W. Zhang, H.-R. Si, Y. Zhu, B. Li, C.-L. Huang, H.-D. Chen, J. Chen, Y. Luo, H. Guo, R.-D. Jiang, M.-Q. Liu, Y. Chen, X.-R. Shen, X. Wang, X.-S. Zheng, K. Zhao, Q.-J. Chen, F. Deng, L.-L. Liu, B. Yan, F.-X. Zhan, Y.-Y. Wang, G.-F. Xiao, Z.-L. Shi, (**2020**) A pneumonia outbreak associated with a new coronavirus of probable bat origin. *Nature,* 579: 270–273.